# High-field spin dynamics of the one-dimensional spin-$\frac{1}{2}$ Heisenberg antiferromagnet $\alpha$-*bis* (N-methylsalicylaldiminato copper) (II) ($\alpha$-CuNSal)

L. J. Azevedo, A. Narath, P. M. Richards, and Z. G. Soos*
*Sandia Laboratories,† Albuquerque, New Mexico 87185*
(Received 30 July 1979)

Proton spin-lattice relaxation rates in the one-dimensional (1D) spin-$\frac{1}{2}$ Heisenberg antiferromagnet $\alpha$-*bis* (N-methylsalicylaldiminato) copper (II), $\alpha$-CuNSal, have been measured in applied fields up to 125 kOe in the temperature range 1–4 K. The strong coupling of protons close to the antiferromagnetic (AF) chain serves as a convenient probe to study the dynamics of the AF chain through the field-induced antiferromagnetic to ferromagnetic (F) phase transition. The magnetization of the AF chain, as measured by the proton field shift, is in close agreement with calculations by Bonner and Fisher and yields an exchange interaction $J/k = 3.04 \pm 0.04$ K. The proton relaxation rate has isotropic (hyperfine coupled) and anisotropic (dipolar) components. We identify the isotropic relaxation rate with a creation or destruction of one-spin excitations (magnons) and the anisotropic rate with two-magnon processes. The measured one-magnon relaxation rate shows an enhancement near the critical field for the AF $\rightarrow$ F transition and a strong decrease of more than four decades as the critical field is exceeded. A no-adjustable-parameter calculation based on the fermion model quantitatively agrees with the measured one-magnon relaxation rate, both above and below the critical field $H_c$. The enhanced relaxation at $H_c$ is correctly predicted as a consequence of the divergence of the 1D density of magnon states, where a gap in the spin-wave spectrum exists. Above $H_c$ a finite magnon lifetime must be included in order to produce a nonzero one-magnon relaxation rate. This is also calculated with no adjustable parameters. The two-magnon relaxation rate also shows a decrease as the critical field is exceeded and the calculated relaxation rate agrees well with experiment at low temperatures, provided, however, that one uses a boson rather than fermion picture.

## I. INTRODUCTION

The transition-metal-ion salt $\alpha$-*bis* (N-methylsalicylaldiminato) copper (II), $\alpha$-CuNSal, is among the best realizations of the one-dimensional (1D) Heisenberg antiferromagnet (AF), whose Hamiltonian in a magnetic field is

$$\mathcal{H} = 2J \sum_n \vec{S}_n \cdot \vec{S}_{n+1} - g_e \mu_B H_0 \sum_n S_n^z \quad . \tag{1}$$

We present here proton NMR results on crystalline $\alpha$-CuNSal at low temperature ($1 < T < 4$ K) and high applied field ($H_0 < 125$ kOe). Although the first term in Eq. (1) describes antiferromagnetic coupling, a sufficiently large $H_0 > H_c = 4J/g_e\mu_B$ can lead to ferromagnetic order. Our principal results are the thorough experimental examination of paramagnetic shifts $\Delta H$ and of longitudinal relaxation times $T_1$ as $H_0$ passes through the region of $H_c$. The theoretical analysis of $\Delta H$ and $T_1$ in this novel low-temperature, high-field regime is developed in terms of the fermion representation for spin flips in the 1DAF.

Much of the analytical work on the spin-$\frac{1}{2}$ 1DAF has been based on the fermion model,[1] which is exact[2] for the anisotropic $XY$ model. It may, therefore, be a convenient starting point for the Heisenberg model, Eq. (1), which has not yet been solved exactly for finite-temperature properties. Numerical analyses of finite rings of $N$ spins together with extrapolation to the $N \rightarrow \infty$ limit have provided useful information about static thermodynamic properties.[2,3] Such coarse-grained calculations are generally ill suited for describing the low-frequency dynamics probed by NMR.

Our results show that excellent agreement with proton relaxation rates is possible at low temperatures both above and below the critical field $H_c$ for ferromagnetic order. This is particularly significant because the NMR relaxation rate $T_1^{-1}$ above $H_c$, where the excitation spectrum has a gap, depends not only on the magnon energies, but also on their lifetimes. Although many of the qualitative features of the $T_1^{-1}$ data can be understood without explicit recourse to the fermion picture, it seems to provide the simplest model for quantitative agreement. A no-adjustable-parameter fit is made possible by a detailed analysis of the angular and field dependence of the proton NMR. Not only are the coupling constants determined, but from the angular dependence of $T_1^{-1}$ we can determine separately the one-magnon and two-

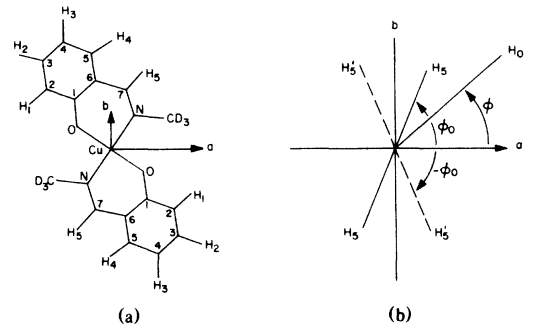


FIG. 1. (a) One molecule of CuNSal. (b) Simplified diagram of position of $H_5$ as discussed in the text. Dotted lines show positions of $H_5$ on adjacent molecules down the stack.

magnon contributions of $T_1^{-1}$. We also compare results obtained in the fermion representation with a boson model. Although the fermion picture is far superior for the dominant (except at very high fields) one-magnon rate, a boson description actually works better for the two-magnon process, which is relatively insensitive to the magnon lifetimes.

The properties of crystalline $\alpha$-CuNSal make it a nearly ideal system for a study of this nature. One molecule of $\alpha$-CuNSal is shown in Fig. 1(a). Each copper (II) has a spin $S=\frac{1}{2}$, and the complexes form stacks along the $c$ axis.[4]

The isotropic exchange interaction is found to be $J/k=3.2\pm0.2$ K from static-susceptibility[5] and from magnetic-specific-heat[6] measurements. The ESR[7] of $\alpha$-CuNSal also points to 1D behavior and is well described by $\mathcal{H}$. The observed three-dimensional ordering[8] in zero field at 0.044 K shows that interactions between CuNSal complexes in different stacks are small.

Electron spin delocalization over a CuNSal molecule leads to hyperfine in addition to dipolar coupling to the proton $H_5$, shown in Fig. (1a). Thus, $H_5$ is a good probe of the spin dynamics of the AF chain. Experimental details are described in Sec. II. The angular, field, and temperature dependence of the paramagnetic shifts $\Delta H$ and the relaxation rate of the $H_5$ proton are described in Sec. III. $T_1$ relaxation in one dimension is discussed in Sec. IV and Sec. V deals with calculation of the magnon relaxation rate.

## II. EXPERIMENTAL

The $\alpha$-CuNSal sample used was a single-crystal needle of 3-mm length and 0.3-mm sides. The methyl protons in Fig. 1 were about 95% deuterated. The crystal was mounted in a single-layer NMR coil of 2-mm length and 0.5-mm internal diameter. The coil winding was enamel-insulated 75-$\mu$m copper wire. The needle axis ($c$ axis) was parallel to the rf field for all experiments. Since the crystal extended out of the coil, its orientation relative to the coil and the $a$, $b$ axes was identified by x-ray diffraction on the mounted crystal. The sample was held in position with a small amount of Apiezon $N$-grease.

The NMR coil was mounted on a rotation apparatus[9] capable of 150° rotations in the $ab$ plane and 90° rotations in any plane containing the $c$ (needle) axis. As a result, we could obtain only partial rotations in any plane containing the $c$ axis. All measurements were performed in a liquid-He bath, with temperature determined by measuring the vapor pressure. The static magnetic field $H_0$ was provided by a $Nb_3Sn$ superconducting solenoid. The available temperature range was $1.08\leq T\leq4.02$ K, and the highest $H_0$ was 125 kOe.

Proton spin-lattice relaxation rates ($T_1^{-1}$) were obtained from a phase-coherent spectrometer[10] whose available frequencies were 2 to 700 MHz. All $T_1$ measurements used a $\frac{1}{2}\pi$ saturating pulse followed by a $\frac{1}{2}\pi-\pi$ pulse pair. The echo amplitude was monitored by a boxcar integrator.[11] Recovery of the nuclear magnetization was exponential over at least $1\frac{1}{2}$ decades.

The error in temperature measurements was $\lesssim2\%$. The error in $H_0$ was $\lesssim10$ Oe, as determined from the unshifted protons in the NMR coil wire insulation and in the $N$-grease. The magnetic field orientation was accurate to $\lesssim0.5°$. Demagnetization fields are estimated to be negligibly small due to the dilute nature of the spin system. The maximum demagnetization field would be $2\pi M=17$ Oe if the sample were a long needle. Although most of our data were taken on a single sample, we have made measurements on several other samples and have observed identical spectra and relaxation rates.

## III. RESULTS

### A. High-field spectrum

The $^1$H absorption spectrum versus $H_0$ is shown in Fig. 2 for several orientations of $H_0$ in the $ab$ plane (Fig. 1) at the resonance frequency of 450 MHz (105.7 kOe) and 1.08 K. The electron spins are 96% saturated, as shown below. We first note that $H_0\parallel a$ or $b$ in Fig. 2 leads to five resolved proton lines corresponding to the five inequivalent protons of a CuNSal complex in Fig. 1(a). The two complexes in the unit cell, shown schematically in Fig. 1(b), are magnetically equivalent for $H_0\parallel a$ or $b$. At other orientations, the complexes are magnetically inequivalent, and each resonance splits into two lines. The coalescence points agree within experimental error with the crystalline $a$ and $b$ axes as found by x-

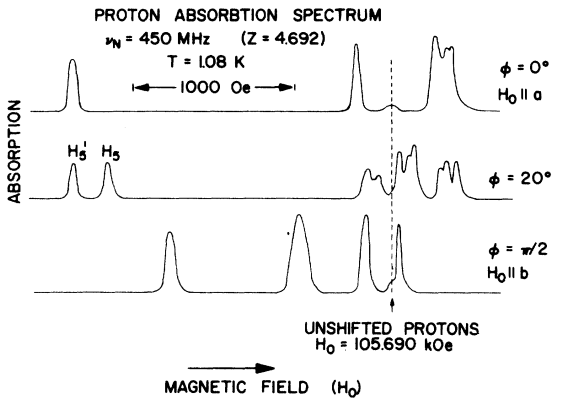


FIG. 2. Proton absorption spectrum vs applied magnetic field. For the field along the crystallographic $a$ or $b$ axes, the spectrum collapses to five lines, corresponding to the five magnetically inequivalent protons in the unit cell. The unshifted proton line is from the coil wire enamel and $N$-grease.

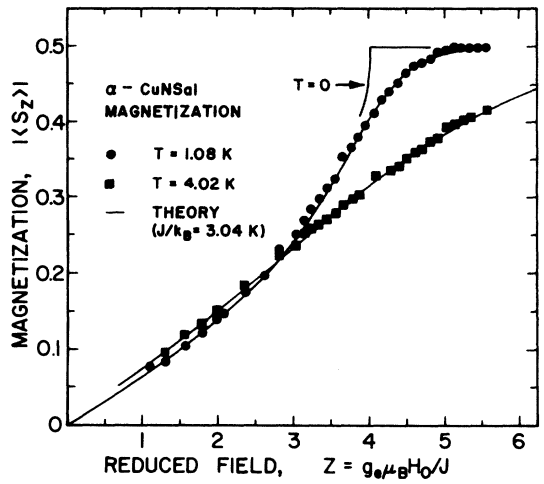


FIG. 3. Magnetization vs reduced field at two temperatures. The solid curves are the one-adjustable-parameter fit of Bonner-Fisher calculations for the magnetization. Note that the magnetization is saturated for $z > 5$ at the lowest temperature.

ray diffraction on the mounted sample.

A weak triplet spectrum corresponding to incomplete deuteration of the methyl protons has been deleted from Fig. 2. The unshifted $^1$H resonance whose position does not depend on the orientation of $H_0$ and whose $T_1$ is very long ( $\sim 60$ sec), is identified as protons in the $N$-grease and in the enamel coil wire insulation. This signal provides a convenient reference for measuring the splittings $\Delta H$ of the other regions.

The final point about Fig. 2 is that the field splittings for protons $H_1$, $H_2$, $H_3$, and $H_4$ (Fig. 1) are small and essentially dipolar in origin, but the splittings for $H_5$ are large and involve both hyperfine and dipolar contributions. Further evidence for spin delocalization to $H_5$ is provided by natural abundance $^{13}$C NMR of $C_7$ and $CD_3$, which are adjacent to N in Fig. 1. Both $C_7$ and $CD_3$ have large saturated hyperfine shifts of 2170 and 2356 Oe, respectively, consistent with spin delocalization over part of the complex.

### B. Magnetization

Paramagnetic shifts are proportional to $\langle S_z \rangle$, the average magnetization of the electron spins in the applied field $H_0$. The shifts $\Delta H$, in units of $g_e\mu_B$, for the $H_5$ protons are shown in Fig. 3 at the lowest (1.08 K) and highest (4.02 K) temperatures versus the reduced magnetic field $z = g_e\mu_B H_0/J$. At 1.08 K the system has clearly been driven completely to ferromagnetic order, or $|\langle S_z \rangle| = \frac{1}{2}$, for $z > 5.2$. This is consistent with the theoretical $T = 0$ result[3] for the Heisenberg antiferromagnet that the critical field occurs at $z = 4$. The only adjustable parameter for analyzing the magnetization by Eq. (1) with a field added is thus the isotropic exchange $J$. The solid curves in Fig. 3 are based on the Bonner-Fisher[3] and Bonner[12] numerical results for finite chains, which are then extrapolated to infinite chains. The best fit at $T = 1.08$ K ($kT/J = 0.36$) yields $J/k = 3.04 \pm 0.04$ K. The same value for $J$ fits the $T = 4.02$ K data in Fig. 3. This value of $J$ is close to the $3.2 \pm 0.2$ K results[5,6] based on the static susceptibility and on the magnetic specific heat. Such close agreement between theory and experiment for static properties has been observed[3] in other 1D systems and affords further experimental verification that $\alpha$-CuNSal is a nearly ideal 1DAF.

The paramagnetic shifts $\Delta H$ for the $H_5$ protons depend on the orientation of $H_0$. The isotropic (or largely hyperfine) and anisotropic (or largely dipolar) contributions in the $ab$ plane were found to have the constant ratio of 2.74 over the entire $H_0$ range in Fig. 3. Since each contribution is proportional to $\langle S_z \rangle$, the constant ratio supports our interpretation that $H$-vs-$z$ curves in fact measure the magnetization of the spin chain.

### C. Angular dependence of $\Delta H$

Although the paramagnetic shifts $\Delta H_5$ for the $H_5$ and $H_5'$ protons can be analyzed for the complete low-temperature crystal structure, it is more instructive to adopt the idealized geometry in Fig. 1. First, we neglect the 4° tilt of the complexes relative to the $c$ (needle) axis and thus ensure that all local magnetic interactions have one principal axis along $c$ and the other two in the $ab$ plane. This is an adequate approximation for all $\Delta H$ and $T_1$ data reported here. The other approximation is to treat the $H_5$-N-Cu-N-

$H_5$ path in Fig. 1 as a straight line. This ensures that the Cu-H and N-H dipolar or hyperfine interactions share common principal axes in the $ab$ plane, at $\phi_0 = 73°$ for $H_5$ and at $\phi_0 = -73°$ for $H_5'$. The unpaired electron density is approximated as usual[13] by $\rho_{Cu} \sim 0.8$ and $\rho_N \sim 0.1$ and all the fractional spins are collinear. The hyperfine and dipolar contributions to $\Delta H$ for the $H_5$ protons involve the $S_z I_z$ terms (with $z$ along $H_0$). Since $g_e = 2.047$ is isotropic in the $ab$ plane, we find

$$\Delta H(\phi - \phi_0) = \langle S_z \rangle \{a_1 \cos^2(\phi - \phi_0) + a_2 \sin^2(\phi - \phi_0) + d[1 - 3\cos^2(\phi - \phi_0)]\} , \quad (2)$$

where $a_1$, $a_2$ are the principal hyperfine strengths in the $ab$ plane, and $d$ is the dipolar interaction, which we simplify as

$$d = \mu_B g_e \left( \frac{\rho_{Cu}}{r_{Cu}^3} + \frac{\rho_N}{r_{1N}^3} + \frac{\rho_N}{r_{2N}^3} \right) . \quad (3)$$

The distances $r_{Cu}$, $r_{1N}$, and $r_{2N}$ between $H_5$ and the copper and two nitrogen atoms, respectively, are known from the structure. Equation (3) is then summed over all CuNSal complexes taking the proper angular dependences.

The angular dependence of $\Delta H(\phi - \phi_0)$ at 1.08 K and 450 MHz is shown in Fig. 4, together with a least-squares fit based on Eq. (2) and 96% magnetization. Note that there are only three independent variables since the angular dependence of the anisotropic hyperfine shift and the dipolar interaction is the same. We assume $a_1 = a_2$ and the fit yields $\phi_0 = 73°$, in agreement with the structural determination of the average Cu-N-$H_5$ angle to the $a$ axis, $a_1 = 5.44 \times 10^{-4}$ cm$^{-1}$ (1915 Oe) and $d = 466$ Oe. We can completely account for $d$ by taking $\rho_{Cu} = 0.77$ and $\rho_N = 0.115$, using Eq. (3), and summing over all CuNSal complexes within a sphere of radius 200 Å.

Moores and Belford[14] studied the ESR of isolated CuNSal complexes in a diamagnetic host with the same structure. They report $H_5$ hyperfine constants of $A_1 = a_1 - 2d = 5.5 \times 10^{-4}$ cm$^{-1}$ and $A_2 = a_2 + d = 4.3 \times 10^{-4}$ cm$^{-1}$, with $\pm 0.2 \times 10^{-4}$-cm$^{-1}$ uncertainties. The magnitudes are in good agreement with our results on the crystalline solid. Since we can completely account for the anisotropy in the field shift by the dipolar interaction with a reasonable choice of $\rho_{Cu}$, the assumption $a_1 = a_2$ is justified. However, we cannot rule out some small anisotropy in the hyperfine interaction of the order 10%, but this small anisotropy will not affect our calculation of the relaxation rates as shown below. We will therefore adopt our best values of $a_1 = a_2 = 5.44 \times 10^{-4}$ cm$^{-1}$ and $d = 466$ Oe in analyzing $T_1$ data with $H_0$ in the $ab$ plane.

### D. $T_1$ relaxation

The angular dependence of $T_1^{-1}$ in the $ab$ plane for the $H_5$ protons is shown in Fig. 5 for several values

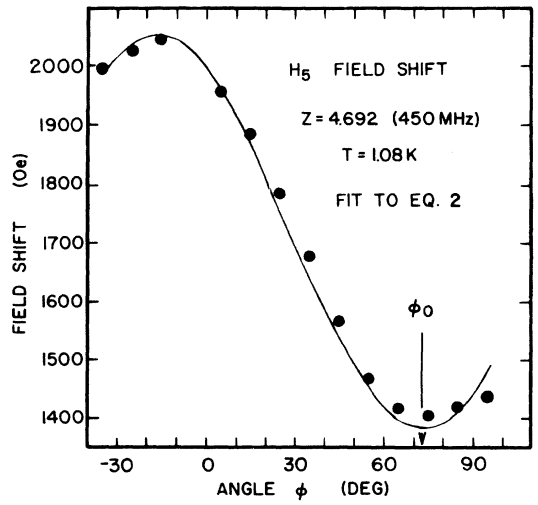


FIG. 4. Proton $H_5$ field splitting vs direction of applied field in the $ab$ plane. The solid line is a least-squares fit to Eq. (2), as discussed in the text.

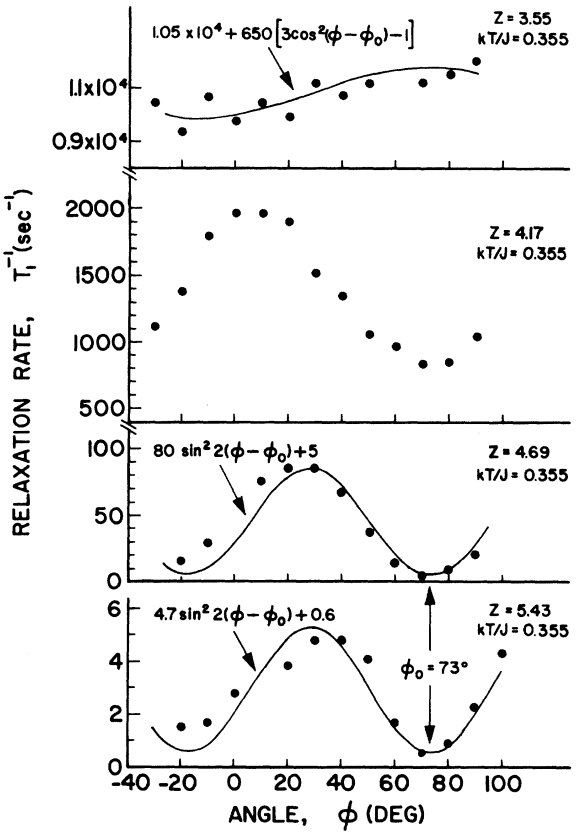


FIG. 5. Spin-lattice relaxation rate of $H_5$ vs angle in the $ab$ plane at several values of applied field. Solid curves are guides to the eye.

of $z = g_e \mu_B H_0 / J$ at 1.08 K. The relaxation rate is greatly reduced for the $H > H_c$ ($z > z_c = 4$) curves. At the highest field, with $z = 5.43$ and $\nu_{NMR} = 520$ MHz, $T_1^{-1}$ goes as $\sin^2 2(\phi - \phi_0)$, as indicated by the solid line in Fig. 5. The minima correspond within experimental error to $\phi_0 = 73°$, the mean Cu-N-$H_5$ direction. The $H_5'$ pattern is out of phase, with minima at $\phi_0 = 73°$, but is otherwise similar.

The $S_z(I^+ + I^-)$ dipolar coupling between the $H_5$ protons and the electronic moment on a CuNSal complex goes as $\sin 2(\phi - \phi_0)$ which would produce $T_1^{-1} \alpha \sin^2 2(\phi - \phi_0)$ when $H_0$ is in the $ab$ plane, whereas an isotropic $a \vec{I} \cdot \vec{S}$ hyperfine interaction gives no angular variation. The $z = 5.43$ data in Fig. 5 thus represent almost pure dipolar coupling due to the $S_z(I^+ + I^-)$ term. As shown in Sec. IV this indicates that two-magnon ($S_z$) terms dominate the high-field relaxation.

At lower $H_0$, other mechanisms must be included. Although all $z \gtrsim 4$ curves in Fig. 5 have the same qualitative angular behavior, the minima in $T_1^{-1}$ at $\phi = 73°$ clearly increase as $z$ is lowered, and an accurate fit to $\sin^2 2(\phi - \phi_0)$ cannot be obtained. For $z < 4$, furthermore, even the qualitative features change. At $z = 3.4$, for example, Fig. 5 shows that the minimum at $\phi = 73°$ has disappeared and that the anisotropy is only about 10%. An isotropic $T_1^{-1}$ results if the isotropic hyperfine interaction dominates the relaxation. As discussed in Sec. IV this is expected for $z < 4$ where there is no gap in the excitation spectrum and one-magnon ($S^+$, $S^-$) terms are the most important.

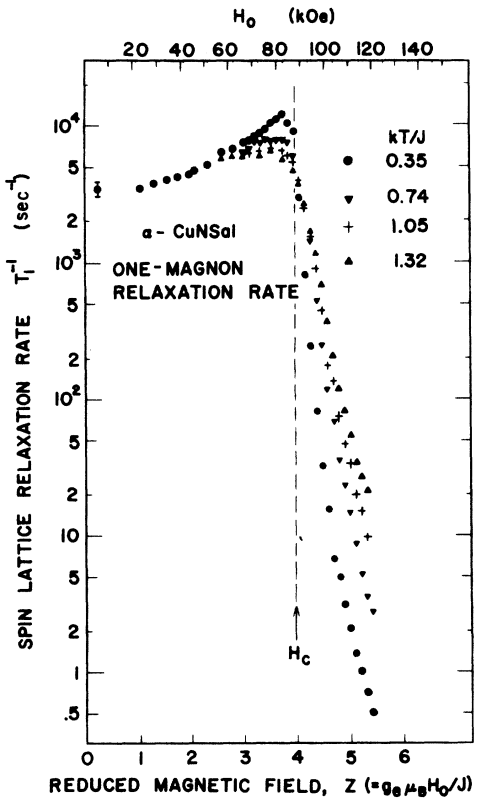


FIG. 6. One-magnon relaxation rate of $H_5$ vs reduced field at several temperatures. Dotted line shows critical field at zero temperature.

The field dependence of $T_1^{-1}$ at $\phi = 73°$, where the $S_z(I^+ + I^-)$ two-magnon term is absent, is shown in Fig. 6 for several temperatures. For $z \lesssim 2.5$, $T_1^{-1}$ is essentially independent of temperature for $0.35 \lesssim kT/J \lesssim 1.3$ and only the $kT/J = 0.35$ results are shown. At the lowest temperature (1.08 K), $T_1^{-1}$ has a maximum at $z \approx 4$ and then decreases by more than four orders of magnitude for $z > 4$. The $T_1^{-1}$ peak around $z \approx 4$ broadens with increasing $T$ and moves to lower field. The decrease in $T_1^{-1}$ for $z > 4$ becomes less pronounced at higher $T$.

## IV. $T_1$ RELAXATION IN ONE DIMENSION

### A. Electron-proton coupling

The paramagnetic shifts $\Delta H$ discussed in Sec. II D indicate that the $H_5$ protons are predominantly coupled to the unpaired electron on the same CuNSal complex, and that the hyperfine coupling exceeds the dipolar interaction. The hyperfine components $a_1$ and $a_2$ in the $ab$ plane are isotropic. The component $a_3$ along the chain is less accurately known and may be somewhat ($\sim 30\%$) smaller. However, since the $H_5$ hyperfine tensor is expected to be approximately collinear with the Cu-N-$H_5$ direction (Fig. 1) of the idealized geometry, we will assume that $a_3$ is also equal to $a_1 = a_2$, so that the hyperfine coupling becomes isotropic $a \vec{I} \cdot \vec{S}$ with $a = 5.44 \times 10^{-4}$ cm$^{-1}$ deduced from the paramagnetic shifts. The dipolar contributions to $\Delta H$ are almost an order of magnitude smaller.

For simplicity, we focus on one of the $H_5$ protons, denoted as $\vec{I}$, at the $n = 1$ CuNSal complex in the infinite cyclic chain. The on-site electron-proton coupling is written conventionally as

$$\mathcal{H}_{e-p} = A_0(\Omega) S_{1z} I_z + \mathcal{H}_1 + \mathcal{H}_2 \ , \tag{4}$$

where $\mathcal{H}_1$ and $\mathcal{H}_2$ represent coupling of $I^{\pm}$ to $S_1^{\pm}$ and $S_1^z$, respectively, which we later identify as one- and two-magnon terms, and $A_0(\Omega)\langle S_z \rangle$ describes the paramagnetic shifts for $\hbar \gamma_N H_0 >> a$. For $a_1 = a_2 = a$ in Eq. (2), the angular dependence of $A_0$ in the $ab$ plane is simply

$$A_0(\Omega) = a + g_n \mu_n d[1 - 3\cos^2(\phi - \phi_0)] \ , \tag{5}$$

with $a = 5.44 \times 10^{-4}$ cm$^{-1}$ (1915 Oe) and $d = 466$ Oe obtained from the $\Delta H$ fit.

The two-magnon term $\mathcal{H}_2$ is purely dipolar as long

as the hyperfine interaction is isotropic

$$\mathcal{H}_2 = A_2(\Omega) S_{1z}(I^+ + I^-) \ , \tag{6}$$

with

$$A_2(\Omega) = \tfrac{3}{4} g_n \mu_n d \sin 2(\phi - \phi_0)$$

in the $ab$ plane. The one-magnon term $\mathcal{H}_1$ involves all $S_1^+$ and $S_1^-$ terms,

$$\mathcal{H}_1 = A_1(\Omega)(S_1^+ I^- + S_1^- I^+) + B_1(\Omega)(S_1^+ I^+ + S_1^- I^-) \ . \tag{7}$$

The angular dependence of the coefficients $A_1(\Omega)$ and $B_1(\Omega)$ in the $ab$ plane is

$$A_1(\Omega) = \tfrac{1}{2} a + \tfrac{1}{4} g_n \mu_n d[3\cos^2(\phi - \phi_0) - 1] \ ,$$
$$B_1(\Omega) = -\tfrac{3}{4} g_n \mu_n d \sin^2(\phi - \phi_0) \ . \tag{8}$$

Similar results can be found for $H_5'$ protons by changing $\phi_0$ to $-\phi_0$.

For a general electron-nuclear coupling of the form $\vec{h}\cdot\vec{I}$, where $\vec{h}$ is an effective field linear in the electron-spin operators, the longitudinal NMR relaxation rate is given by[15]

$$T_1^{-1} = \tfrac{1}{2}\hbar^{-2} \mathrm{Re} \int_0^\infty dt [\langle h_+(t) h_-(0)\rangle + \langle h_-(t) h_+(0)\rangle - 2\langle h_+\rangle \langle h_-\rangle] \ . \tag{9}$$

Here $h_\pm = h_x \pm i h_y$, angle brackets indicate a thermal average, "Re" stands for real part, and time dependence $h_\pm(t)$ arises from damping and precession of the electronic spin in the exchange Hamiltonian [Eq. (1)]. The quantity $2\langle h_+\rangle \langle h_-\rangle$ appears in Eq. (9) to guarantee that the time correlation functions decay to zero as $t \to \infty$. It is assumed that the time dependence of $\langle h_\pm(t) h_\mp(0)\rangle$ is at a rate much more rapid than the NMR frequency $\omega_n$ so that $\exp(\pm i\omega_n t)$ factors may be replaced by unity. This is reasonable since, even at the highest $H_0$, the nuclear energy $\hbar\omega_N \leq 25$ mK is negligible compared with the magnon bandwidth $4J \approx 12$ K. Comparison with Eqs. (6) and (7) shows that

$$h_\pm = 2[A_2(\Omega) S_1^z + A_1(\Omega) S_1^\pm + B_1(\Omega) S_1^\pm] \ . \tag{10}$$

From Eqs. (9) and (10) we see that $T_1^{-1}$ is determined by the near-zero-frequency spectral density of the longitudinal and transverse ($S_1^\pm$) electron-spin operators. This spectral density is evaluated within the context of the fermion model as outlined below.

### B. Fermion representation

There have been several treatments[16–18] of the spin-$\frac{1}{2}$ Heisenberg chain by the fermion model. We summarize here those features of the random-phase-approximation (RPA) fermion calculation that are needed to compute the spectral densities for NMR relaxation. Fermion creation and annihilation operators $a_n^\dagger$ and $a_n$ are associated with $S_n^+$ and $S_n^-$ according to

$$S_n^+ = (-1)^{\sigma_n} a_n^\dagger \ , \tag{11a}$$

$$S_n^- = (-1)^{\sigma_n} a_n \ , \tag{11b}$$

where the phase factors

$$\sigma_n = \sum_{j=1}^{n-1} a_j^\dagger a_j \tag{12}$$

ensure that fermion operators on different sites anticommute, even though the spin operators for different sites commute. The transformation holds for any $S = \frac{1}{2}$ spin system, although the phase factors $\sigma_n$ only simplify in one dimension. The $z$ component of spin is then related to the number operator by

$$S_{nz} = -\tfrac{1}{2} + a_n^\dagger a_n \ . \tag{13}$$

The vacuum state $|0\rangle$ has all spins with $S_{nz} = -\frac{1}{2}$ and is the exact ground state for $H_0 > H_c$. The total $z$ component $S_z$, which is conserved since $[\mathcal{H}, S_z] = [\mathcal{H}, S^2] = 0$, then measures the number of fermions, or spin deviations above $|0\rangle$. For $H_0 = 0$, the exact ground state of $\mathcal{H}$ is a singlet. There are $\frac{1}{2}N$ fermions and $S_z = 0$. However, the total spin $S$ must usually be approximated in the fermion picture, and this is one of its defects.

The $S_n^z S_{n+1}^z$ part of $\mathcal{H}$ leads to interactions between fermions, thereby precluding an exact analysis. The Hamiltonian Eq. (1) now reads[16]

$$\frac{\mathcal{H}}{J} = \tfrac{1}{2} N(1 - z) + \sum_k (z - 2 + 2\cos k) a_k^\dagger a_k + \frac{2}{N} \sum_{qkk'} \cos q \, a_{k+q}^\dagger a_{k'-q}^\dagger a_{k'} a_k \ , \tag{14}$$

where $z = g_e \mu_B H_0 / J$ is the reduced field, the fermions $a_k^\dagger, a_k$ are Fourier transforms of $a_n^\dagger, a_n$, and the wave vector $k$ is in the first Brillouin zone, $-\pi < k < \pi$. Various molecular field (RPA) solutions[16–18] of Eq. (6) are generally close to numerical results for static properties.

The excitations (magnons) induced by $a_k^\dagger$ form a 1D band of $N$ states, as shown in Fig. 7, with RPA energies[16]

$$\frac{\epsilon_k}{J} = z - 4s + 2p\cos k \ , \tag{15}$$

where

$$s = |\langle S_z\rangle| = \frac{1}{2} - \frac{1}{N} \sum_k n_k \tag{16}$$

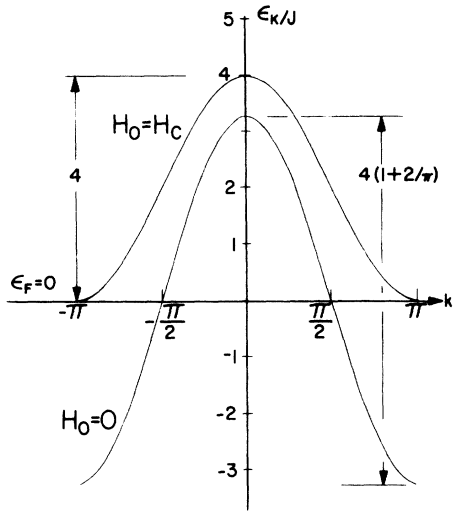


FIG. 7. Excitation spectrum for magnons at $H_0=0$ and $H_0=H_c$. States are occupied up to the Fermi level $\epsilon_F$.

and $p$ is a bandwidth parameter

$$p=1-\frac{2}{N}\sum_k n_k \cos k \quad . \tag{17}$$

Equations (16) and (17) are solved self-consistently with the occupation number $n_k$ given by Fermi statistics as

$$n_k=[\exp(\beta\epsilon_k)+1]^{-1} \tag{18}$$

$$(\beta=1/kT) \quad .$$

We have $s=\frac{1}{2}$ and $p=1$ for $z\geq 4$ and $T=0$ K, while $z=0$ leads to $s=0$ and $p=1+2/\pi$.

As shown in Fig. 7, the Fermi energy at zero temperature is always at $\epsilon_F=0$. The $H_0=0$ band is half filled, with $\frac{1}{2}N$ spin deviations, while the band is empty for $H_0>H_c$ and there is an energy gap of $J(z-4)$ even for the zone-edge magnons at $k=\pm\pi$. The normalized density of states $\rho(\epsilon)$, with $\epsilon=\epsilon_k/J$, is found from Eq. (15) to be

$$\rho(\epsilon)=\frac{1}{\pi J}[4p^2-(\epsilon-z+4s)^2]^{-1/2} \quad , \tag{19}$$

for $z-4s-2p<\epsilon<z-4s+2p$ and zero otherwise. All negative $\epsilon_k$ are occupied at 0 K, and these spin reversals for $z<4$ determine the magnetization.

One can show that the transformation in Eq. (11) is valid for a cyclic ring[2] where all spins must have equivalent properties. One is therefore at liberty to focus on $n=1$ for discussing the dynamics of a single electron spin on the ring. There the phase factors are unity, giving a one-to-one correspondence between transverse-spin and fermion operators. It is then evident that the perturbation $\mathcal{H}_1$ of Eq. (7) involves one-magnon relaxation and $\mathcal{H}_2$ of Eq. (6) is a two-magnon term. Note also that within the fermion picture there are *no* higher-order magnon terms, as opposed to the Holstein-Primakoff transformation[19] where transverse-spin operators contain all odd-order magnon terms.

Detailed calculations of the one- and two-magnon rates are presented in Sec. IV C, but some qualitative remarks may be made here. Nuclear relaxation via two magnons (coupling to $S_1^z$) involves the annihilation of a spin deviation of $k'$ and its recreation with wave vector $k$. The difference in magnon energy is the nuclear energy $\hbar\omega_n$, which is generally negligible in comparison to the electronic bandwidth of $\sim 4J$. The temperature dependence of $S_n^z$ or two-magnon processes is thus controlled by the Fermi-Dirac probability of having an occupied and empty fermion level at almost the same energy. The one-magnon (coupling to $S_1^{\pm}$) processes, by contrast, involve a single excitation whose energy must be essentially zero in order to induce a spin flip at $\hbar\omega_n$. At low temperature, one-magnon processes are proportional to the density of states at zero energy for $H_0<H_c(z<4)$. They probe the magnon lifetimes $\Gamma_k^{-1}$ for $H_0>H_c$, since they can only occur for $z>z_c$ by virtue of the lifetime broadening of the magnon energies. The different temperature dependence of one- and two-magnon $T_1^{-1}$ relaxation is clearly shown by the $H_5$ protons of $\alpha$-CuNSal.

The advantages of single-crystal studies are now apparent. The angular dependence of the paramagnetic shifts $\Delta H$ of the $H_5$ and $H_5'$ protons in Sec. IV directly yields the coupling constants for the electron-proton interaction. The angular dependence of $T_1^{-1}$ then immediately identifies $S_z$, or two-magnon, processes for $z>4$. There are consequently *no* adjustable parameters left in analyzing the field and temperature dependence of the nuclear relaxation $T_1$, and one can compare theory with experiment for the one- and two-magnon rates separately.

### C. One-magnon relaxation rate

The one-magnon relaxation rate is given by the transverse operators of $h_{\pm}$ in Eqs. (9) and (10) which are then converted to fermion operators. The result is

$$(T_1^{-1})_1=2\hbar^{-2}N^{-1}[A_1^2(\Omega)+B_1^2(\Omega)]\,\mathrm{Re}\sum_k\int_0^{\infty}dt\,\langle a_k^{\dagger}(t)a_k(0)+a_k(t)a_k^{\dagger}(0)\rangle \quad . \tag{20}$$

Axial symmetry of the electronic Hamiltonian has been noted so that terms $\langle S_1^{\pm}(t)S_1^{\pm}(0)\rangle$ are identically zero.

We assume that

$$\langle a_k^\dagger(t)a_k(0)\rangle = \langle a_k^\dagger a_k\rangle e^{i\omega_k t}e^{-\Gamma_k t} = n_k e^{i\omega_k t}e^{-\Gamma_k t} , \quad (21a)$$

$$\langle a_k(t)a_k^\dagger(0)\rangle = \langle a_k a_k^\dagger\rangle e^{-i\omega_k t}e^{-\Gamma_k t} = (1-n_k)e^{-i\omega_k t}e^{-\Gamma_k t} , \quad (21b)$$

where $\omega_k = \epsilon_k/\hbar$ with $\epsilon_k$ the magnon energy of Eq. (15); $n_k$ is the occupation number given by Eq. (18), and $\Gamma_k$ is a damping constant to be calculated later. Insertion of Eqs. (21) into (20) then gives

$$(T_1^{-1})_1 = \frac{2}{N\hbar^2}[A_1^2(\Omega)+B_1^2(\Omega)]\sum_k \frac{\Gamma_k}{\omega_k^2+\Gamma_k^2} . \quad (22)$$

Note that a feature of the fermion representation is that the strongly temperature-dependent occupation numbers cancel because the expression (20) calls for occupation of state $k$ by *either* a particle or hole. This has been noted in a previous treatment[20] of the low-temperature zero-field relaxation rate.

The expression (22) together with the spectrum Eq. (15) shows that the $T\to 0$ relaxation rate is strongly field dependent above and in the vicinity of $H_c(z \gtrsim 4)$. Consider first $z<4$. In this case there is a finite density of states at $\omega_k = 0$ so that, assuming small $\Gamma_k$, we have

$$(T_1^{-1})_1 = \frac{2\pi}{N\hbar^2}[A_1^2(\Omega)+B_1^2(\Omega)]\sum_k \delta(\omega_k) = \frac{2\pi}{\hbar}[A_1^2(\Omega)+B_1^2(\Omega)]\rho(0) , \quad (23)$$

where $\rho(\epsilon_k) = \pi^{-1}dk/d\epsilon_k$ is the normalized density of states. Thus, the one-magnon rate for $z<4 (H_0<H_c)$ is given by the familiar golden rule with a fermion density of states.

The small angular dependence in the $z=3.55$ curve of Fig. 5 can therefore be understood as the $(\frac{1}{2}a)^2$ and $\frac{1}{4}g_n\mu_n$ ad $[3\cos^2(\phi-\phi_0)-1]$ cross terms of $A_1^2$ in Eq. (8) since for $a^2 >> g_n^2\mu_n^2 d^2$ the one-magnon process is dominant at low fields.

The $\epsilon=0$ density of states $\rho(0)$ drops to zero for $z>4$ and thus the expression (23), which neglects lifetime effects, gives a zero relaxation rate for $z>4$. The more complete Eq. (22) must then be used. We assume that the dominant contribution to the summand comes near $k=\pi$ where the gap $\omega_\pi = \hbar^{-1}J(z-4)$ opens up at $T=0$ for $z>4$. A first approximation is then to take

$$(T_1^{-1})_1 \approx 2\Gamma\hbar^{-1}[A_1^2(\Omega)+B_1^2(\Omega)]\int_{z-4}^{z}\frac{\rho(\epsilon)d\epsilon}{\epsilon^2+\Gamma^2} , \quad (24)$$

where $\Gamma$ is the zone-edge damping constant in units of $J/\hbar$. The integral can be evaluated if we assume that it converges for $\epsilon << z\ (z>4)$ so that the upper limit is extended to infinity and $\epsilon << z$ assumed in the density-of-states expression (19). The result is

$$(T_1^{-1})_1 \approx \frac{[A_1^2(\Omega)+B_1^2(\Omega)]}{\hbar J}\left[\frac{(x^2+\Gamma^2)^{1/2}-x}{2(x+4)(x^2+\Gamma^2)}\right]^{1/2} , \quad (25)$$

where $x = z-4 > 0$.

In Fig. 8 we show the $T=0$ behavior of $(T_1^{-1})_1$, which reflects the one-magnon density of states. For $H << H_c$ excellent (within 50%) agreement is obtained with the experimental data at $T=1.08$ K using no adjustable parameters (the coupling constants and $J$ are taken from the shifts $\Delta H$). In Eq. (25) we take

$$\Gamma = (2\pi)^{-1}\left(\frac{kT}{J}\right)^2 e^{-\beta J(z-4)} ,$$

as derived in Sec. V, [see Eq. (41)] for $T=1.08$ K. A more complete numerical calculation is presented in Sec. V.

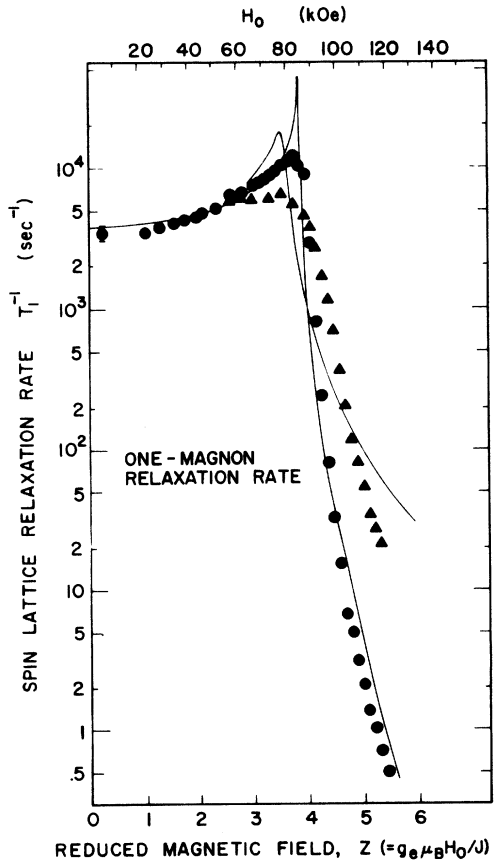


FIG. 8. One-magnon relaxation rate of $H_5$ vs reduced field for $T=1.08$ K (●) and $T=4.02$ K (▲). Solid lines are no-adjustable-parameter theory as discussed in text.

### D. Two-magnon relaxation rate

From Eqs. (9), (10), and (13) the two-magnon ($S_1^z$) relaxation rate is

$$(T_1^{-1})_{II}=4\frac{A_2^2(\Omega)}{\hbar^2N^2}\sum_{k_1k_2k_3k_4}\mathrm{Re}\int_0^\infty dt[\langle a_{k_1}^\dagger(t)a_{k_2}(t)a_{k_3}^\dagger(0)a_{k_4}(0)\rangle-\langle a_{k_1}^\dagger a_{k_2}\rangle\langle a_{k_3}^\dagger a_{k_4}\rangle]$$

$$=\frac{4A_2^2(\Omega)}{\hbar^2N^2}\sum_{k_1k_2}n_{k_1}(1-n_{k_2})\frac{\Gamma_{k_1}+\Gamma_{k_2}}{(\omega_{k_1}-\omega_{k_2})^2+(\Gamma_{k_1}+\Gamma_{k_2})^2}\ . \tag{26}$$

If the resonance term is replaced by a $\delta$ function, one obtains

$$(T_1^{-1})_{II}=\frac{4\pi A_2^2(\Omega)}{\hbar^2}\times\int d\epsilon\, n(\epsilon)[1-n(\epsilon)][\rho(\epsilon)]^2\ , \tag{27}$$

which may be seen from Eq. (19) to result in a logarithmic divergence owing to the 1D character which enhances divergences and the fact that the density of states is squared in the integrand of Eq. (27). Thus, the damping constant must be retained. Note that here letting $\Gamma\to0$ produces an infinite relaxation rate, whereas in the one-magnon case $\Gamma\to0$ gave zero relaxation above $H_c$. In the limit of small damping, the resonance expression

$$(\Gamma_{k_1}+\Gamma_{k_2})/[(\omega_{k_1}-\omega_{k_2})^2+(\Gamma_{k_1}+\Gamma_{k_2})^2]\ ,$$

is sharply peaked at $k_2=k_1$ so that we may approximate Eq. (26) by

$$(T_1^{-1})_{II}=\frac{2A_2^2(\Omega)}{\hbar^2Jp\pi^2}\int_0^\pi dk_1\, n_{k_1}(1-n_{k_1})G(k_1)\ , \tag{28}$$

where

$$G(k_1)=\int_{k_1-\pi}^{k_1}\frac{\eta_{k_1}dy}{(\frac{1}{2}y^2\cos k_1-y\sin k_1)^2+\eta_{k_1}^2}\ , \tag{29}$$

with $\eta_{k_1}=\Gamma_{k_1}/Jp$. We have taken $\Gamma_{k_2}\approx\Gamma_{k_1}$, $n_{k_2}\approx n_{k_1}$, and

$$\omega_{k_1}-\omega_{k_2}=2Jp(\cos k_1-\cos k_2)$$

$$\approx2Jp(\tfrac{1}{2}y^2\cos k_1-y\sin k_1)$$

and $k_2=k_1-y$. This is justified as long as $\Gamma_k\hbar \ll kT$, which [see Eq. (41)] is valid at low temperatures. The integral $G(k_1)$ may be done exactly, and the resulting integration of Eq. (28) performed numerically. The results of this are shown in Fig. 9 where $\Gamma_{k_1}$ is taken from the calculation of Sec. V.

At high fields and low temperatures, where the two-magnon process is most important, the integrand in Eq. (28) is strongly peaked at $k_1=\pi$ and the occupation number $n_{k_1}$ may be approximated by an exponential. In this case, a valid approximation to Eq. (28) is

$$(T_1^{-1})_{II}\approx\frac{A_2^2(\Omega)}{\pi\hbar J}e^{-\beta J(z-4)}\ln(\tfrac{1}{2}\beta J\Gamma)\ . \tag{30}$$

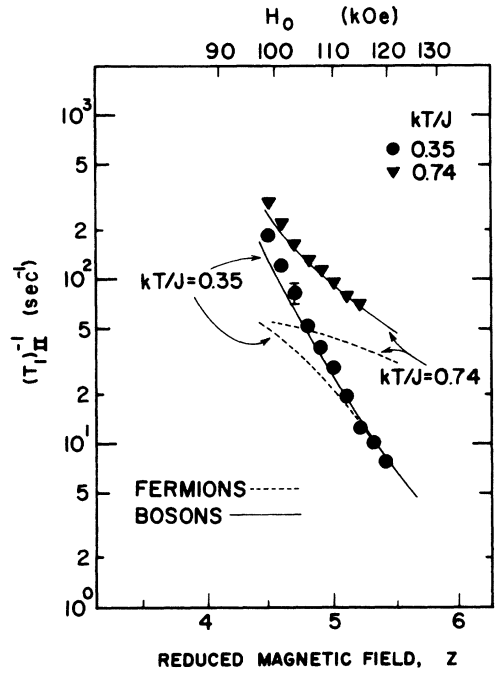


FIG. 9. Two-magnon relaxation rate of $H_5$ vs reduced field for the two lowest temperatures. Curves are the no adjustable theory for fermions and bosons as discussed in text. Please note that there is a plotting error in Fig. 2 of Ref. 22.

## V. MAGNON RELAXATION RATE

Both the one- and two-magnon contributions to $T_1^{-1}$ depend on the inverse magnon lifetime $\Gamma_k$. Simple energy-conserving $\delta$-function approximations give either divergences or zeros in $T_1^{-1}$ except for the one-magnon rate below $H_c$. Here we calculate $\Gamma_k$ by

using time-dependent perturbation theory on the interacting-fermion Hamiltonian of Eq. (14). The perturbation $\mathcal{H}'$ is taken as the non-Hartree-Fock (or nonrandom-phase) part so that we rewrite Eq. (14) as

$$\mathcal{H} = \sum_k \epsilon_k a_k^\dagger a_k + \mathcal{H}' = \mathcal{H}_0 + \mathcal{H}' \ , \tag{31}$$

with

$$\mathcal{H}' = 2JN^{-1} {\sum_{q,k,k'}}' \cos q a_{k+q}^\dagger a_{k'-q}^\dagger a_{k'} a_k \tag{32}$$

and $\epsilon_k$ given by Eq. (15). The constant term in Eq. (14) has been ignored and the prime on the summation sign in Eq. (32) means that RPA terms $q=0, \pm(k-k')$ are excluded. The equation of motion

$$\begin{aligned} \dot{a}_k^\dagger &= i\hbar^{-1}[\mathcal{H}, a_k^\dagger] \\ &= i\omega_k a_k^\dagger + 4iJN^{-1} {\sum_{k',q}}' \cos q \ a_{k+q} a_{k'-q}^\dagger a_{k'}^\dagger \ , \end{aligned} \tag{33}$$

with $\omega_k = \epsilon_k/\hbar$, is rewritten as

$$\dot{\tilde{a}}_k^\dagger = 4iJN^{-1} {\sum_{k',q}}' \cos q \ \tilde{a}_{k+q}^\dagger \tilde{a}_{k'-q}^\dagger \tilde{a}_{k'} \exp[i\Omega(k,k',q)t] \ , \tag{34}$$

where $\tilde{a}_k^\dagger$, $\tilde{a}_k$ are the "interaction representation" values

$$\tilde{a}_k^\dagger = e^{-i\mathcal{H}_0 t/\hbar} a_k^\dagger e^{i\mathcal{H}_0 t/\hbar} = e^{-i\omega_k t} a_k^\dagger \ , \tag{35a}$$

$$\tilde{a}_k = e^{-i\mathcal{H}_0 t/\hbar} a_k e^{i\mathcal{H}_0 t/\hbar} = e^{i\omega_k t} a_k \ , \tag{35b}$$

and

$$\begin{aligned} \Omega(k,k',q) &\equiv \omega_{k+q} + \omega_{k'-q} - \omega_k - \omega_{k'} \\ &= 2Jp[\cos(k+q) + \cos(k'-q) \\ &\quad - \cos k - \cos k'] \ . \end{aligned} \tag{36}$$

As is common practice in time-dependent perturbation theory, we iterate Eq. (34) twice and obtain an expression valid to second order in $\mathcal{H}'$ for the correlation $\langle \tilde{a}_k^\dagger(t) \ \tilde{a}_k(0) \rangle$:

$$\langle \tilde{a}_k^\dagger(t) \tilde{a}_k(0) \rangle \approx n_k(1-\Gamma_k t) \approx n_k e^{-\Gamma_k t} \ . \tag{37}$$

The damping constant $\Gamma_k$ is given explicitly as

$$\Gamma_k = 16J^2N^{-2} \sum_{k',q} \cos q[\cos q - \cos(k+q-k')][n_{k'}(1-n_{k'-q}) + n_{k+q}n_{k'-q} - n_{k+q}n_{k'}] \lim_{\Delta\to 0}\left(\frac{\Delta}{\Omega(k,k',q)^2+\Delta^2}\right) \ . \tag{38}$$

Details of the derivation of Eq. (38) may be found in Appendix.

We replace the double summation in Eq. (38) by a double integral and note that for a continuous density of states ($N\to\infty$) the restrictions $q\neq 0, \pm(k-k')$ may be removed apart from corrections of the order of $1/N$. The integral is sharply peaked at $\Omega(k,k',q)=0$ which occurs for $q=0, k'-k$, and $k'=\pi-k$, and we assume the major contributions come from these regions. In the limit $\Delta\to 0$, we find

$$\begin{aligned} \Gamma_k \approx{}& \frac{2J}{p\pi} \int_{-\pi}^{\pi} dk' \, n_{k'}(1-n_{k'}) \frac{[1-\cos(k-k')]^2}{|\sin k' - \sin k|} \\ &+ \frac{2J}{p\pi} \int_{-\pi}^{\pi} dq[n_{\pi-k}(1-n_{\pi-q}) + n_q n_{\pi-q} - n_q n_{\pi-k}] \frac{[\cos^2(k-q) + \cos(k-q)\cos(k+q)]}{|\sin q - \sin k|} \ . \end{aligned} \tag{39}$$

It is evident that the integrals in Eq. (39) contain logarithmic divergences and thus cannot be evaluated as they stand. A self-consistent solution would put explicit damping in the right-hand side of Eq. (34) by making the replacement

$$\Omega(k,k',q) \to \Omega(k,k',q) + i(\Gamma_{k+q} + \Gamma_{k'-q} + \Gamma_{k'} - \Gamma_k) \ .$$

The quantity $\Delta$ in Eq. (38) then becomes $\Gamma_{k+q} + \Gamma_{k'-q} + \Gamma_{k'} - \Gamma_k$ so one no longer takes the limit $\Delta\to 0$, and finds a contribution of the order of $n_{\pi-k}(1-n_{\pi-k})\ln(1/\Gamma)$ from the divergent regions $k'=\pi-k$, $q=k$, $q=\pi-k$ {there is no divergence at $k'=k$ because of the $[1-\cos(k-k')]^2$ term in the numerator of the first integral in Eq. (39)}. For the $T_1$ calculations we are primarily concerned with $\Gamma_k$ for $k\approx k_F$. Furthermore, only $k_F\approx\pi$ is of great interest since the damping constant is important only for fields near and above $H_c(z=4)$ and $k_F=\pi$ for $z\geq 4$. The one-magnon rate is insensitive to $\Gamma_k$ at low fields where $k_F\approx\frac{1}{2}\pi$ and the two-magnon rate is observable only for $z\geq 4$. Hence, the logarithmic correction is negligible at low temperatures where

$$n_0(1-n_0) \ll \langle n_{k'}(1-n_{k'}) \rangle_{\rm av}$$

and $\langle \ \rangle_{\rm av}$ is an average over the zone. Similar reasoning shows that the second integral in Eq. (39) (that over $dq$) should be negligible compared with the first one at low temperatures for $k\approx k_F\approx\pi$.

In light of the above comments, Eq. (39) is therefore approximated by

$$\Gamma_{k^*} \approx \frac{2J}{p\pi}\int_{-\pi/2}^{\pi/2} dy\, n_{k_F-y}(1-n_{k_F-y}) \times \frac{[1-\cos(k^*-y)]^2}{|\sin(k_F-y)-\sin(k_F-k^*)|} \quad , \tag{40}$$

where $k^* = k_F - k$ and the expression is expected to be valid at low temperature for $\frac{3}{4}\pi \leq k_F \leq \pi$ and $|k^*| \lesssim \frac{1}{2}k_F$. The limits have been taken as $\pm\frac{1}{2}\pi$ so as to stay safely away from the divergences which occur at $\pm\pi$ for $k = k_F = \pi$. Since the population factor

$$n_{k_F-y}(1-n_{k_F-y})$$

decreases rapidly with $y$, the integral should be insensitive to the limits as long as they are well removed from the divergences.

For $H > H_c$ and $k = k_F = \pi$ in the low-temperature limit ($p=1$, $s=\frac{1}{2}$), we may take

$$n_{k_F-y}(1-n_{k_F-y}) \approx n_{k_F-y} \approx \exp[-\beta J(z-4) - \beta J y^2] \quad ,$$

approximate the trigonometric expressions by their $y \ll 1$ values, then extend the limits to $\pm\infty$ and thereby obtain

$$\Gamma_\pi \approx \frac{J}{\pi} e^{-\beta J(z-4)} \int_0^\infty y^3 e^{-\beta J y^2} dy = \frac{J}{2\pi}(\beta J)^{-2} e^{-\beta J(z-4)} \quad . \tag{41}$$

For $\beta J(1-\cos k^*)^2 \geq 1$, we approximate Eq. (40) by taking $y=0$ in the trigonometric functions so that

$$\Gamma_{k^*} \approx \frac{2J}{p\pi}\frac{(1-\cos k^*)^2}{|\sin k_F - \sin(k_F-k^*)|} \times \int_{-\pi/2}^{\pi/2} dy\, n_{k_F-y}(1-n_{k_F-y}) \quad , \tag{42}$$

for sufficiently large $k^*$. This predicts

$$\Gamma_{k^*} \propto T^{1/2}|k^*|^3 e^{-\beta J(z-4)}$$

for $H > H_c$ and $k^* \ll 1$ at low temperature compared with $\Gamma_{k_F} \propto T^2 e^{-\beta J(z-4)}$ from Eq. (41).

It is, of course, unrealistic to assume the $|k^*|^3$ dependence holds all the way to the zone edge, and it is difficult to obtain an analytic expression for $\Gamma_{k^*}$ except in the vicinity of $k^*=0$ because of the logarithmic corrections. Since we expect the integrals in Eqs. (22) and (28) to be dominated by the behavior near $k_F$ and since it seems likely that a truly correct calculation of $\Gamma_k$ may not show such a strong variation away from $k_F$, we use $\Gamma_k = \Gamma_{k_F}$ throughout the zone in the ensuing calculations of $T_1^{-1}$ with $\Gamma_{k_F}$ given by Eq. (40) for $k^*=0$. The nature of the approximations also suggests that Eq. (40) works best at $k^*=0$ for low temperatures and $H > H_c$.

## VI. RESULTS AND DISCUSSION

NMR work by Jeandey *et al.*[21] on powdered $\alpha$-CuNSal at 300 K has shown that the powder-averaged relaxation rate of protons follows $T_1^{-1} \propto \omega_N^{-1/2}$ from 15–200 MHz. Their results are interpreted as a 1D spin-diffusion process. Our results in the temperature range 1–4 K show that $T_1^{-1}$ is independent of frequency between 25 and 100 MHz for the one-magnon relaxation rate of $H_5$. We see no evidence for 1D diffusion in the low-temperature range, and the complete frequency dependence can be understood on the basis of the AF $\rightarrow$ F phase transition. This suggests, as is reasonable, that the spin dynamics of the AF chain are governed by diffusive processes only for $T \gg J/k$.

At high temperatures, the fluctuation spectrum near zero frequency is dominated by the slowly decaying modes $\langle S_k^+(t)S_k^-(0)\rangle$ which are diffusive for $k \rightarrow 0$. These models have greatly reduced amplitude at low temperature where the $k \approx \pi$ modes are favored because of the large staggered (AF) susceptibility, and the magnon-excitation picture becomes appropriate. It should be mentioned that a curious feature of the fermion picture is that, although $\langle S_k^+(t)S_k^-(0)\rangle$ is a constant of the motion at $k=0$ for the Heisenberg magnet in zero field, the same is not true of the fermion correlation $\langle a_k^\dagger(t)a_k(0)\rangle$ at $k=0$. Thus, one should not expect the fermion picture to describe relaxation processes which are dominated by behavior of the *spin* operators near $k=0$. The situation is somewhat mitigated by the fact, as noted earlier, that $\sum_k \langle S_k^+(t)S_k^-(0)\rangle$ is equal to $\sum_k \langle a_k^\dagger(t)a_k(0)\rangle$ even though the relation does not hold for individual $k$'s.

It is interesting to note that our value of $T_1^{-1}|_I = 3.4\times10^3\ s^{-1}$ in the low-field regime is near the value reported by Jeandey *et al.* at low $\omega_N$ of $\sim 2.4\times 10^3\ s^{-1}$. However, there is a basic difference between their room-temperature measurements and our low-temperature ones: We are able to resolve the individual protons and report data for the relaxation of only the strongly coupled $H_5$'s. Such resolution is not possible at high temperature, and the nonexponential decay observed by Jeandey *et al.* contains contributions from all the inequivalent protons. This obviously complicates the analysis and makes quantitative comparison with theory difficult, especially since, as we have shown, the strong coupling of the

$H_5$ protons to the electronic spin is decidedly nondipolar, a fact which was not accounted for in Ref. 21. Hence, the agreement between our $(T_1^{-1})_1$ for $H_5$ and that of Jeandey *et al.* which is some kind of a weighted average, may be purely coincidental.

In Fig. 8 we show results of the no-adjustable-parameter theory for the one-magnon process [Eqs. (22) and (40) with $\Gamma_k = \Gamma_{k_F}$] for the $kT/J = 0.35$ and 1.32 data. There is very good quantitative agreement between theory and experiment over the complete field range for the low-temperature data. Note that the agreement is over more than four decades in the relaxation rate. Other relaxation mechanisms for the proton $H_5$ are estimated to be much smaller than the slowest rate shown in Fig. 8 because the nondipolar relaxation rate of protons $H_1$–$H_4$, which are not hyperfine coupled to the electronic spin, exhibit very long relaxation times. The fit of the $kT/J = 1.32$ theory is not as good as the low-temperature data but certainly reflects qualitatively the measured relaxation rates. The disagreement at higher temperature perhaps reflects the reduction of the (low-temperature-favored) $k = \pi$ modes as noted above or the fact that the perturbation calculation of $\Gamma_{k_F}$ is expected to be less reliable at higher temperatures.

The two-magnon relaxation rate for the two lowest temperatures along with theory is shown in Fig. 9. Due to the large contribution of the one-magnon rate at lower fields and higher temperatures, we only have data for $z \gtrsim 4.5$ at the lower temperatures. The agreement with theory is quite good at the highest field but the observed field dependence is clearly much stronger than calculated. This is puzzling since the two-magnon rate is relatively insensitive to $\Gamma_k$ so that the discrepancy seems to indicate that a description of the process in terms of Fermi factors is inadequate. Indeed, we find that a boson description, shown by the labeled curve in Fig. 9, gives far better agreement. That is, in the expression $S_i^z = S - n_i$, we regard $n_i$ as a boson, rather than fermion, number operator and calculate the spin-wave spectrum using the Holstein-Primakoff transformation to lowest order. The resulting $\epsilon_k$ is the same as for the fermion description in the low-temperature, high-field limit. Consequently the boson curve is obtained simply by changing $1 - n_{k_1}$ to $1 + n_{k_1}$ in Eq. (28) and $n_k$ to $(e^{\beta\epsilon_k} - 1)^{-1}$ in Eq. (18) to give the well-known expression for the two-magnon (Raman) relaxation rate for bosons. In this way we obtain the excellent agreement shown. It is much better than indicated by Fig. 2 of our earlier report[22] which was plotted incorrectly.

## VII. CONCLUSIONS

In conclusion, we find that the fermion picture gives a quantitative, no-adjustable-parameter fit to the one-magnon relaxation rate of proton $H_5$. The divergence of the 1D magnon density of states is clearly seen by the enhancement of $T_1^{-1}$ at the critical field, and the lifetime broadening of the magnon energies, within the fermion picture, fully accounts for the observed field dependence of the one-magnon rate. However, a boson picture appears to give a better description of the two-magnon rate.[22] The fermion model is obviously needed for the low-field, one-magnon rate since the boson formulation would produce a strong temperature dependence which is not observed.[20] Neither the fermion nor the boson model is exact for the Heisenberg model. Further, the one-magnon rate is strongly dependent on the magnon lifetime $\Gamma_k^{-1}$ and—at least within the framework of a single golden rule calculation — is much better described in the fermion picture. We find that a boson golden-rule-type theory predicts a $\Gamma_k$ which is very large at $k = \pi$ and leads to a much weaker field dependence of the one-magnon rate than is observed above the critical field.

One might expect the fermion picture to be valid for the transverse fluctuations in high fields since, with longitudinal $\langle S_i^z(t) S_i^z(0) \rangle$ fluctuations suppressed by the field, the transverse dynamics may be similar to those of the $XY$ model which are given exactly by noninteracting fermions. This is consistent with the good agreement of the one-magnon rate, which involves transverse fluctuations, with fermion theory. The two-magnon rate is given by longitudinal fluctuations, and it is not at all clear that these should be described by a fermion calculation. An *a posteriori* conclusion is that they are much better treated by lowest-order Holstein-Primakoff theory. We have no explanation, however, how this could have been anticipated *a priori*.

## ACKNOWLEDGMENTS

We would like to thank B. Morosin for the x-ray orientation of the samples. One of us (Z.G.S.) would like to thank Sandia for summer support. We acknowledge helpful discussions with M. A. Butler, B. Morosin, W. G. Clark, P. Pincus, D. Hone, and J. C. Bonner. Also, many thanks to J. C. Bonner for providing magnetization curves for the 1D antiferromagnet. We also acknowledge the technical assistance of R. L. White. This work was supported by the U. S. DOE under Contract No. DE-AC04-76-DP00789.

## APPENDIX

We outline here the steps involved in going from Eq. (34) to Eqs. (38) and (39). First, rewrite Eq. (34) as

$$\dot{a}_k^\dagger = i \sum_{k',q}{}' L(k,k',q;t) \exp[i\,\Omega(k,k',q)\,t] \quad , \qquad \text{(A1)}$$

where

$$L(k,k',q;t) = 4JN^{-1}\tilde{a}^{\dagger}_{k+q}(t)\,\tilde{a}^{\dagger}_{k-q}(t)\,\tilde{a}_{k'}(t) \quad . \tag{A2}$$

With the identity

$$f(t) = f(0) + \int_0^t \dot{f}(t_1)\,dt_1 \quad ,$$

we have

$$\begin{aligned}\tilde{a}^{\dagger}_k(t) &= \tilde{a}^{\dagger}_k(0) + i\int_0^t dt_1 \sum_{k',q}{}' L(k,k',q;t_1)\exp[i\Omega(k,k',q)t_1] \\ &= \tilde{a}^{\dagger}_k(0) + i\int_0^t dt_1\, L(k,k',q;0)\exp[i\Omega(k,k',q)t_1] + i\int_0^t dt_1 \int_0^{t_1} dt_2 \sum_{k',q}{}' \dot{L}(k,k',q;t_2)\exp[i\Omega(k,k',q)t_1] \quad .\end{aligned} \tag{A3}$$

The derivative $\dot{L}(k,k',q;t_2)$ is obtained by differentiating Eq. (A2) according to Eq. (33) and its Hermitian conjugate. Thus,

$$\begin{aligned}L(k,k',q;t_2) = 4iJN^{-1} \sum_{k',q}{}' \cos q \sum_{k'',q}{}' \{ & L(k+q,k'',q',t_2)\tilde{a}^{\dagger}_{k'-q}\tilde{a}_{k'}\exp[i\Omega(k+q,k'',q')t_2] \\ & + \tilde{a}^{\dagger}_{k+q}L(k'-q,k'',q';t_2)\tilde{a}_k\exp[i\Omega(k+q,k'',q')t_2] \\ & - \tilde{a}^{\dagger}_{k+q}\tilde{a}^{\dagger}_{k'-q}L^{\dagger}(k',k'',q';t_2)\exp[-i\Omega(k',k'',q')t_2]\} \quad .\end{aligned} \tag{A4}$$

We then make the usual approximation of assuming that $\tilde{a}^{\dagger}_k$, $\tilde{a}_k$ are slowly varying compared with the exponential time factors which appear explicitly in Eq. (A3) and (A4) so that the $L$'s, $a$'s and $a^{\dagger}$'s on the right-hand side of Eq. (A4) are at $t=0$. The correlation function $\langle \tilde{a}_k{}^{\dagger}(t)\,\tilde{a}_k(0)\rangle$ is of primary interest. Use of Eq. (A4) in the second equality of Eq. (A3) gives

$$\begin{aligned}\langle \tilde{a}^{\dagger}_k(t)a_k(0)\rangle = n_k - 16J^2N^{-2}\sum_{k',q}{}' \cos q\,[\cos q - \cos(k+q-k')]\,n_k\,[n_{k'}(1-n_{k'-q}) + n_{k+q}n_{k'-q'} - n_{k+q}n_{k'}] \\ \times \int_0^t dt_1 \int_0^{t_1} dt_2 \exp[i\Omega(k,k',q)(t_1-t_2)]\exp[-\Delta(t_1-t_2)] \quad ,\end{aligned} \tag{A5}$$

where $n_k = \langle \tilde{a}^{\dagger}_k(0)\,\tilde{a}_k(0)\rangle = \langle a^{\dagger}_k\,a_k\rangle$, and an imaginary part $\Delta$ has been added to $\Omega(k,k',q)$ which will later be let to approach zero.

In arriving at Eq. (A5), we have assumed that an average such as

$$\langle \tilde{a}^{\dagger}_{k_1}(0)\tilde{a}^{\dagger}_{k_2}(0)\tilde{a}^{\dagger}_{k_3}(0)\tilde{a}_{k_4}(0)\tilde{a}_{k_5}(0)\tilde{a}_{k_6}(0)\rangle = \langle a^{\dagger}_{k_1}a^{\dagger}_{k_2}a^{\dagger}_{k_3}a_{k_4}a_{k_5}a_{k_6}\rangle \quad ,$$

may be computed by RPA and thus reduces to

$$\begin{aligned}n_{k_1}n_{k_2}n_{k_3}[&\delta_{1,4}(\delta_{3,5}\delta_{2,6} - \delta_{2,5}\delta_{3,6}) \\ &+ \delta_{1,5}(\delta_{2,4}\delta_{3,6} - \delta_{2,6}\delta_{3,4}) \\ &+ \delta_{1,6}(\delta_{2,5}\delta_{3,4} - \delta_{2,4}\delta_{3,5})] \quad ,\end{aligned}$$

for $k_1 \neq k_2 \neq k_3$ where $\delta_{ij}$ is the Kronecker $\delta$ for $k_i = k_j$.

The integral I in Eq. (A5) is transformed to

$$\mathrm{I} = \int_0^t (t-\tau)\exp[i\Omega(k,k',q)\tau]e^{-\Delta\tau}d\tau \quad , \tag{A6}$$

with $\tau = t_1 - t_2$. The "long-time short-time" approximation is then employed whereby one assumes that $t$ is sufficiently long that $t \gg \tau$ for the value of $\tau$ for which the integral is non-negligible and thus the upper limit extended to $\infty$ so that

$$\mathrm{I} \approx t\int_0^{\infty} \exp[i\Omega(k,k',q)\tau]e^{-\Delta\tau}d\tau \quad . \tag{A7}$$

The time $t$ is regarded, however, as sufficiently short that the resulting second term on the right-hand side of Eq. (A5) $n_k\Gamma_k t$ is much less than $n_k$, whence $\Gamma_k$ may be seen to agree with the expression given in Eq. (39) (only the real part of I has been taken since a small frequency shift is not of interest). In this case, the first equality in Eq. (39) is taken as the leading terms in an expansion of $e^{-\Gamma_k t}$.

Equation (20) shows that we are interested in $\int_0^{\infty} dt\,\langle a^{\dagger}_k(t)a_k(0)\rangle$, i.e., the zero-frequency component, for calculation of the one-magnon contribution to $T_1^{-1}$. In addition to the above, which, in combination with Eq. (22), expresses the $\omega = 0$ component in terms of a damping constant $\Gamma_k$, there is a

competing process which gives rise to an $\omega=0$ component. It is equivalent to the virtual magnon scattering discussed by Beeman and Pincus[23] and comes about as follows: With the help of Eq. (35) we may rewrite Eq. (A5) as

$$\langle a_k^\dagger(t)a_k(0)\rangle = n_k e^{i\omega_k t} - \sum_{k',q}{}' G(k,k',q)e^{i\omega_{k'}t}\mathrm{I} \ , \quad \text{(A8)}$$

where I is the integral defined in Eq. (A6) and $G(k,k',q)$ is the coefficient of I in Eq. (A5). Complete evaluation of I rather than the approximation of Eq. (A7) gives

$$\mathrm{I} = \frac{it}{\Omega(k,k',q)+i\Delta} + \frac{1}{[\Omega(k,k',q)+i\Delta]^2} - \frac{\exp[i\Omega(k,k_1,q)t]e^{-\Delta t}}{[\Omega(k,k',q)+i\Delta]^2} \ . \quad \text{(A9)}$$

The first term in Eq. (A9) is the same as Eq. (A7) and produces the damping constant already discussed. The second term gives only a small amplitude shift and is no consequence here. The third term contributes to $\int_0^\infty dt\,\langle a_k^\dagger(t)a_k(0)\rangle$ an amount

$$K = \sum_{k',q}{}' \frac{G(k,k',q)}{(\Omega(k,k',q)+i\Delta)^2} \times \int_0^\infty \exp\{i[\Omega(k,k_1,q)+\omega_k+i\Delta]t\}\,dt$$

$$= \frac{\pi}{\omega_k^2}\sum_{k',q}{}' G(k,k',q)\delta[\Omega(k,k',q)+\omega_k] \ , \quad \text{(A10)}$$

where we have taken $\Delta\to 0$ and neglected the imaginary part which leads to a frequency shift. If we utilize the definition Eq. (36) of $\Omega(k,k',q)$ and note the previous expression for $\Gamma_k$ it follows that

$$\int_0^\infty dt\,\langle a_k^\dagger(t)a_k(0)\rangle = \frac{n_k\Gamma_k}{\omega_k^2} + K = \frac{\pi}{\omega_k^2}\sum_{k',q}{}' G(k,k',q)[\delta(\omega_{k+q}+\omega_{k'-q}-\omega_k-\omega_{k'})+\delta(\omega_{k+q}+\omega_{k'-q}-\omega_{k'})] \ , \quad \text{(A11)}$$

where we have assumed $\Gamma_k \ll \omega_k$ in the first term on the right-hand side of the first equality and ignored the logarithmic divergences associated with taking $\Delta=0$. The first term on the right-hand side of the second equality in Eq. (A11) is the contribution from $\Gamma_k$, while the second is the Beeman-Pincus (BP) term. Note that they differ only in the energy-conserving $\delta$ functions, the former involving four magnons and the latter three magnons. Although we have not evaluated the three-magnon BP term explicitly, it seems reasonable that it should be smaller than the $\Gamma_k$ contribution on the general grounds that the geometry is more restrictive for three-magnon energy conservation. For example, there can be no three-magnon terms for $H > 2H_c$ since we require

$$H - 2J = 2J(\cos k_2 + \cos k_3 - \cos k_1) \ , \quad \text{(A12)}$$

for the $k_1 \to k_2 + k_3$ process at 0 K in high fields according to the spectrum Eq. (15). The largest value the right-hand side of Eq. (A12) can attain is $6J$, and thus the process is not possible for $H > 8J = 2H_c$. We therefore expect the BP process to be negligible at least for sufficiently high fields.

*Permanent address: Dept. of Chemistry, Princeton University, Princeton, NJ 08540
†U. S. DOE facility.

[1]S. Rodriguez, Phys. Rev. 116, 1474 (1959).
[2]J. I. Krugler, C. G. Montgomery, and H. M. McConnell, J. Chem. Phys. 41, 2421 (1964); S. Katsura, Phys. Rev. 127, 1508 (1962); E. Lieb, T. D. Schultz, and D. C. Mattis, Ann. Phys. 16, 407 (1961).
[3]J. C. Bonner and M. E. Fisher, Phys. Rev. 135, A 640 (1964).
[4]E. C. Lingafelter, G. L. Simmons, B. Morosin, C. Scheringer, and C. Freiburg, Acta Crystallogr. 14, 1222 (1961).
[5]R. C. Knauer and R. R. Bartkowski, Phys. Rev. B 7, 450 (1973).
[6]L. J. Azevedo, W. G. Clark, D. Hulin, and E. O. McLean, Phys. Lett. A 58, 255 (1976).
[7]R. R. Bartkowski and B. Morosin, Phys. Rev. B 6, 4209 (1972).
[8]L. J. Azevedo, W. G. Clark, and E. O. McLean, in *Proceedings of the Fourteenth International Conference on Low Temperature Physics LT14, Otaniemi, Finland, 1975*, edited by M. Krusius and M. Vuorio (North-Holland, Amsterdam, 1975), p. 369; L. J. Azevedo, Ph.D. thesis (U.C.L.A., 1975) (unpublished).
[9]L. J. Azevedo, Rev. Sci. Instrum. 50, 231 (1979).
[10]A. Narath and D. C. Barham, Rev. Sci. Instrum. 45, 100 (1974).
[11]W. G. Clark, Rev. Sci. Instrum. 35, 316 (1964).
[12]J. C. Bonner (private communication).
[13]B. R. McGarvey, in *Proceedings of the Symposium on Electron Spin Resonance of Metal Chelates, Pittsburgh Conference on Analytical Chemistry and Applied Spectroscopy, Cleveland, Ohio, March 1968*, edited by Teh Yen (Plenum, New York, 1969), p. 1.
[14]B. W. Moores and R. L. Belford, in *Proceedings of the Sym-*

*posium on Electron Spin Resonance Metal Chelates, Pittsburgh Conference on Analytical Chemistry and Applied Spectroscopy, Cleveland, Ohio, March 1968*, edited by Teh Yen (Plenum, New York, 1969), p. 13.
[15]See, for example, C. P. Slichter, *Principles of Magnetic Resonance* (Harper and Row, New York, 1963), pp. 148–152.
[16]L. N. Bulaevskii, Sov. Phys. JETP 16, 685 (1963).
[17]S. Inawashiro and S. Katsura, Phys. Rev. 140, A 892 (1965).
[18]A. J. Silverstein and Z. G. Soos, J. Chem. Phys. 53, 326 (1970).
[19]T. Holstein and H. Primakoff, Phys. Rev. 58, 1098 (1940).
[20]E. Ehrenfreund, E. F. Rybaczewski, A. F. Garito, A. J. Heeger, and P. Pincus, Phys. Rev. B 7, 421 (1973).
[21]C. Jeandey, J. P. Boucher, F. Ferrieu, and M. Nechtschein, Solid State Commun. 23, 673 (1977).
[22]L. J. Azevedo, A. Narath, P. M. Richards, and Z. G. Soos, Phys. Rev. Lett. 43, 875 (1979).
[23]D. Beeman and P. Pincus, Phys. Rev. 166, 359 (1968).